ARTICLE OPEN

Check for updates

Electronic nature of the pseudogap in electron-doped Sr_2IrO_4

Shuting Peng[1,8], Christopher Lane[2,8], Yong Hu[1,8], Mingyao Guo[1,8], Xiang Chen[3], Zeliang Sun[1], Makoto Hashimoto[4], Donghui Lu[4], Zhi-Xun Shen[5], Tao Wu[1], Xianhui Chen[1], Robert S. Markiewicz[6], Yao Wang[7], Arun Bansil[6], Stephen D. Wilson[3] and Junfeng He[1]✉

In high-temperature (T_c) cuprate superconductors, many exotic phenomena are rooted in the enigmatic pseudogap state, which has been interpreted as consisting of preformed Cooper pairs or competing orders or a combination thereof. Observation of pseudogap phenomenologically in electron-doped Sr_2IrO_4—the 5d electron counterpart of the cuprates, has spurred intense interest in the strontium iridates as a testbed for exploring the exotic physics of the cuprates. Here, we examine the pseudogap state of electron-doped Sr_2IrO_4 by angle-resolved photoemission spectroscopy (ARPES) and parallel theoretical modeling. Our analysis demonstrates that the pseudogap state of Sr_2IrO_4 appears without breaking the particle–hole symmetry or inducing spectral broadening which are telltale signatures of competing orders in the cuprates. We find quasiparticle dispersion and its temperature dependence in the pseudogap state of Sr_2IrO_4 to point to an electronic order with a zero scattering wave vector and limited correlation length. Particle–hole symmetric preformed Cooper pairs are discussed as a viable mechanism for such an electronic order. The potential roles of incommensurate density waves are also discussed.

npj Quantum Materials (2022)7:58 ; https://doi.org/10.1038/s41535-022-00467-1

INTRODUCTION

The pseudogap state in high-T_c cuprate superconductors has been a central issue in condensed matter physics[1–11]. Sr_2IrO_4 is a pseudospin-1/2 Mott insulator that can be described by the same minimal model as the cuprates, and the appearance of the mysterious pseudogap phase in this non-cuprate system has been the subject of much recent attention[12–23]. Significance of the pseudogap in the electron-doped Sr_2IrO_4, however, depends on the nature of this gapped state and the extent to which it drives a generic ordering tendency rooted in the shared minimal model, and provides the basis for a wealth of emergent phenomena, including high-T_c superconductivity[14–25].

RESULTS

Spectroscopic characteristics of the pseudogap state

Insight into the character of the pseudogap state can be obtained by scrutinizing the form of gap opening in the electronic band dispersion[3–11]. Accordingly, we have carried out photoemission measurements along the antinodal high-symmetry direction of an electron-doped Sr_2IrO_4 crystal (Fig. 1, Supplementary Fig. 1), where the pseudogap effect was observed to reach its maximum in the momentum space[12,13]. The electron doping is realized by potassium surface deposition on a La-doped Sr_2IrO_4 sample (Supplementary Fig. 2). At high temperature (150 K), when the pseudogap is absent, we see a single band crossing the Fermi level (E_F) at two different momentum points (Fig. 1a, d). This is consistent with our tight-binding calculations of the band structure (Fig. 1i and Supplementary Fig. 3) which provide a gapless starting point for investigating the pseudogap state. But, at low temperature (30 K), the dispersion bends back without crossing the Fermi level and gives rise to the pseudogap (Fig. 1e–h). A careful examination of the spectra reveals the following characteristics: (1) the top of the band is not at (π,0) in the gapped state (compare Fig. 1a, b with Fig. 1e, f). (2) The back-bending behavior of the dispersion is clear, but it displays a small curvature (Fig. 1e, f, j), such that the absolute value of the electron velocity in the back-bending region is much smaller than that in the original band. (3) The back-bending momenta in the gapped state [marked by the dark red energy distribution curves (EDCs) in Fig. 1e] are aligned with the Fermi momenta (K_F1 and K_F2) defined in the gapless normal state (dark red EDCs in Fig. 1a). The preceding points can also be quantitatively visualized by tracing the energy positions of the EDC intensity maxima as a function of momentum at different temperatures. Results are shown in Fig. 1j, where the low-temperature gap minimum (~30 meV) is identified at the high-temperature Fermi momenta (marked by the dashed lines). This energy gap gradually decreases with increasing temperature and disappears between 120 K and 150 K (Fig. 1j and Fig. 2a–c).

Besides the distinctive band dispersion associated with the pseudogap state, the nature of the pseudogap is also encoded in the spectral line shape[10,26]. For this purpose, the temperature evolution of the EDC at the Fermi momentum (K_F1) is shown in Fig. 2a, b. While the opening of the pseudogap initially depletes the spectral weight at the Fermi level, a sharp quasiparticle peak starts to emerge in the vicinity of the gap at low temperatures (e.g. at 30 K, see Fig. 2a, b). The full-width-at-half-maximum (FWHM) of the peak is extracted and shown in Fig. 2d. It decreases monotonically with decreasing temperature, indicating a reduced scattering rate in the low-temperature regime. The effective single-particle scattering rate (Γ) can also be obtained by fitting

[1]Department of Physics and CAS Key Laboratory of Strongly-coupled Quantum Matter Physics, University of Science and Technology of China, 230026 Hefei, Anhui, China. [2]Theoretical Division and Center for Integrated Nanotechnologies (CINT-LANL), Los Alamos National Laboratory, Los Alamos, NM 87545, USA. [3]Materials Department, University of California, Santa Barbara, CA 93106, USA. [4]Stanford Synchrotron Radiation Lightsource, SLAC National Accelerator Laboratory, Menlo Park, CA 94025, USA. [5]Stanford Institute for Materials and Energy Sciences, SLAC National Laboratory, and Departments of Physics and Applied Physics, Stanford University, Stanford, CA 94305, USA. [6]Department of Physics, Northeastern University, Boston, MA 02115, USA. [7]Department of Physics and Astronomy, Clemson University, Clemson, SC 29631, USA. [8]These authors contributed equally: Shuting Peng, Christopher Lane, Yong Hu, Mingyao Guo. ✉email: jfhe@ustc.edu.cn

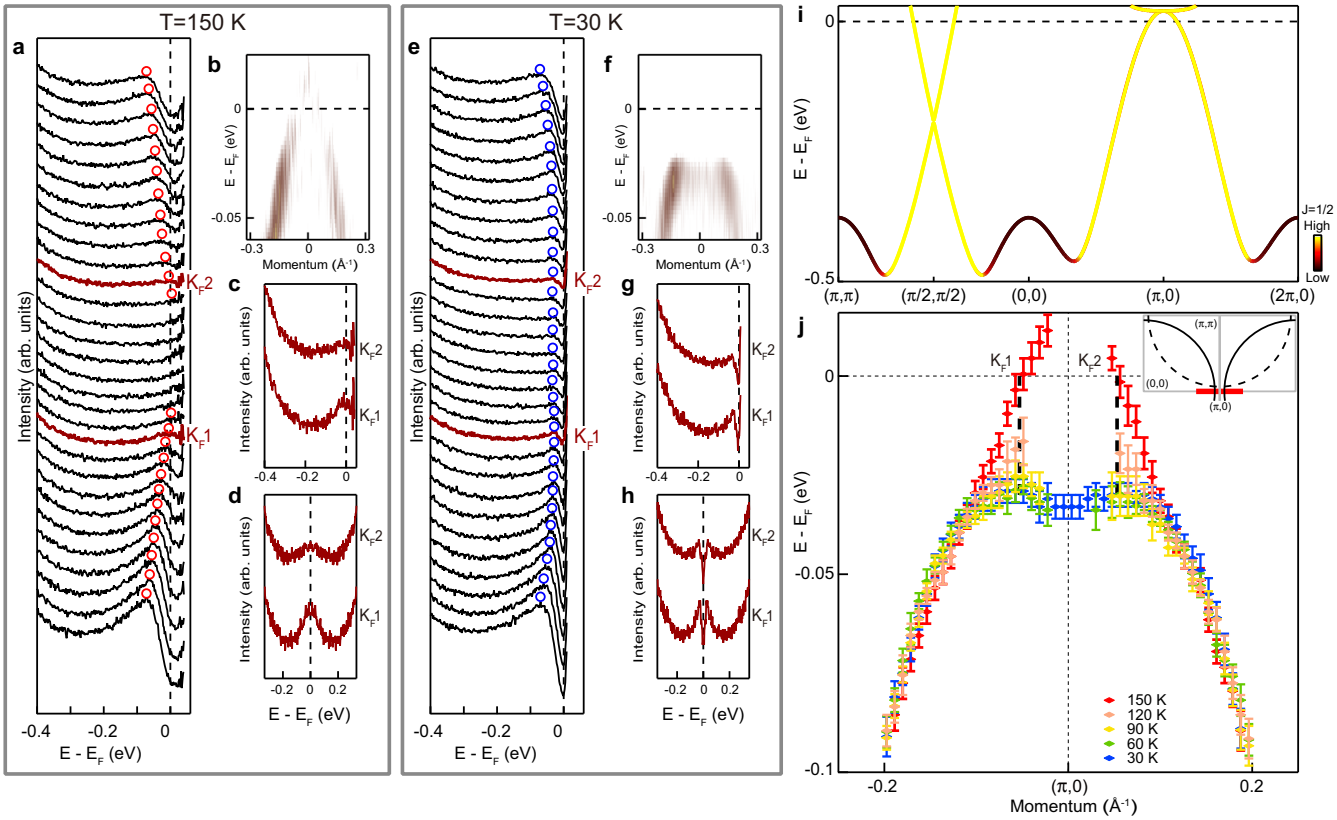

Fig. 1 Temperature dependence of the antinodal band dispersion in electron-doped Sr_2IrO_4. a Raw EDCs of the photoemission spectrum along the antinodal cut divided by the Fermi–Dirac function at 150 K. EDC peak positions are marked by the red circles. The two EDCs at the Fermi momenta are shown in dark red and labeled as K_F1 and K_F2. **b** Second derivative image with respect to the energy of the antinodal dispersion at 150 K. **c**, **d** The Fermi–Dirac-function-divided (**c**) and symmetrized (**d**) EDCs at K_F1 and K_F2, shown on an expanded scale. **e**–**h**, Same as **a**–**d**, but measured at 30 K. **i** Calculated band dispersions along the high-symmetry directions. The color bar represents the relative weight of $J = 1/2$ to $J = 3/2$ states. **j** Dispersion of the intensity maximum as a function of temperature. The energy error bars represent uncertainties in the determination of the EDC peak positions. The momentum error bars are smaller than the size of the symbol. The curvature of the back-bending behavior at low temperature is small, which also gives rise to some uncertainty in the determination of the exact back-bending position. With this error bar, the back-bending momenta measured at several low temperatures are aligned with the Fermi momenta measured at high temperature. The location of the antinodal momentum cut is shown in the inset. Potassium surface deposition was applied to the La-doped sample $(Sr_{1-x}La_x)_2IrO_4$ ($x \sim 0.048$) to achieve a high electron doping level (Supplementary Fig. 2), where the appearance of low-temperature quasiparticles enables a quantitative determination of the dispersion in the pseudogap state. An undistorted Brillouin zone is used to make a direct comparison with the cuprates.

the data to a phenomenological model[27], which shows a similar temperature evolution as that of the extracted FWHM (Fig. 2d).

DISCUSSION

After establishing the spectroscopic characteristics of the pseudogap state of electron-doped Sr_2IrO_4 (also see Supplementary Fig. 4), we now compare them with the cuprates and the results of some model calculations to gain insight into their origin. Density-wave orders have been proposed to account for the pseudogap in cupates[6–10]. With finite scattering wave vectors, these orders would break the particle–hole symmetry and typically compete with superconductivity[10,11]. Photoemission measurements on Bi2201 ($Pb_{0.55}Bi_{1.5}Sr_{1.6}La_{0.4}CuO_{6+\delta}$) have revealed such particle–hole symmetry breaking as well as spectral broadening with decreasing temperature in its pseudogap phase, supporting the density-wave scenario[10]. Various density-wave orders have also been reported in electron-doped Sr_2IrO_4[18,19,21,22], making them natural candidates for the observed pseudogap. However, for a typical density-wave order, the finite scattering wave vector would push the back-bending momenta away from the Fermi momenta[10] (e.g., see Fig. 3b for the simulated photoemission spectrum for a [π,π] density-wave order, also see Supplementary Fig. 5), which is inconsistent with our data (Fig. 3a). One exception is a stripe order with a special wave vector **Q** that connects the two Fermi momenta in the normal state (Fig. 3c). In this case, although the particle–hole symmetry is broken, the back-bending momenta in the gapped state are roughly the same as the Fermi momenta (Fig. 3c). This scenario seems to be compatible with the momentum-alignment observed in our measurements (Fig. 3a). However, there are key differences as follows. First, the calculated gap near E_F (Fig. 3c) is due to hybridization between the main band and the Umklapp bands (main band shifted by ±**Q**). But such Umklapp bands are absent in our experiments, see Supplementary Fig. 6 for details. This result is repeatable on different ARPES systems with different experimental geometry, photon energy and light polarization. Therefore, the absence of the Umklapp bands is intrinsic and not associated with ARPES matrix element effects. Second, due to the scattering process with the wave vector **Q**, the slope of the back-bending region near (π,0) should roughly follow that of the main band (Fig. 3c and Supplementary Fig. 7), which is much steeper than the experimental observation (Fig. 3a). Third, besides the gap at E_F, the hybridization will also produce several energy gaps below E_F (Fig. 3c), which are not seen in our experiments. In addition to the discrepancies in the band dispersion, the temperature evolution of the spectral line width

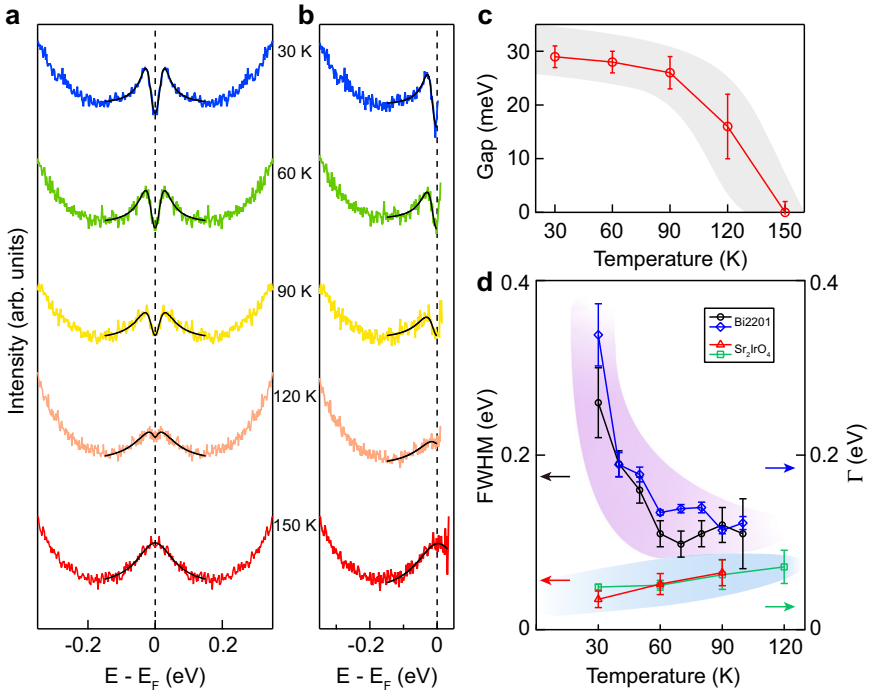

Fig. 2 Temperature evolution of the EDC at the Fermi momentum. a, **b** The symmetrized (**a**) and Fermi–Dirac-function-divided (**b**) EDC at the Fermi momentum K_F1 (defined in Fig. 1), measured at selected temperatures. Fitting results are shown as black lines. The observed quasiparticle peaks at low temperature enable a quantitative determination of the gap. **c** Gap magnitude as a function of temperature. The gray shading is a guide to the eye. **d** Extracted FWHM of the EDC peak (red triangles) and the single-particle scattering rate (Γ) from the fits (green rectangles) are presented as a function of temperature. The same quantities for Bi2201 are extracted from ref. [10] and shown here (black circles and blue diamonds) for comparison. Note that the fitting parameter Γ is only used as an independent but empirical estimation of the EDC peak width; this phenomenological model might not be sufficient to describe the experimental spectra and the results of ref. [10]. The error bars represent the uncertainty in extracting the FWHM of the EDC peak and in the fitting process.

in electron-doped Sr_2IrO_4 is also different from that observed in the cuprate Bi2201 (ref. [10]). As shown in Fig. 2d, the observed sharpening of the quasiparticle peak with decreasing temperature in our experiment is distinct from the competing-order-induced spectral broadening in Bi2201, so that it will be hard to use the same density-wave order to explain the pseudogap state of electron-doped Sr_2IrO_4.

Since the experimental observations cannot be explained by the simple density-wave scenarios with a finite **Q**, we next consider an electronic order with zero scattering wave vector (**Q** = 0). The existence of such an order requires an order parameter not commuting with the Hamiltonian when all sites are summed over. Therefore, neither charge nor spin can form an order with **Q** = 0 in the single-band model. An excitonic order with **Q** = 0 may exist, but it requires the particle and hole to reside in two different bands, which is not the case in Sr_2IrO_4. The textbook example of an order with **Q** = 0 is the BCS superconductivity in which the Bogoliubov quasiparticle exhibits particle–hole symmetry. As shown in Fig. 3d, the back-bending momenta in the superconducting state are perfectly aligned with the Fermi momenta in the normal state. The slope of the back-bending region near (π,0) is very gentle, mimicking that in the experiment. However, the superconducting scenario also has problems. First, no transport evidence for superconductivity has ever been reported in doped Sr_2IrO_4, although spectroscopic indications have been reported on surface-doped samples, possibly due to a higher doping level than the bulk doping limit[16,17,21]. Second, the gap-closing temperature in our experiment is between 120 and 150 K, which is comparable to the highest T_c in the cuprates. However, possible superconductivity in electron-doped Sr_2IrO_4, if any, is predicted to appear at a much lower temperature than that in the cuprates due to a smaller on-site Coulomb repulsion[14,15]. Third, although the energy gap starts to appear at 120 K, the quasiparticle peak remains very weak until a much lower temperature is reached (Fig. 2). This is distinct from the superconducting state, where the apparent Bogoliubov quasiparticles should appear with the superconducting gap.

A model considering the **Q** = 0 order with a limited correlation length might better capture the experimental results. In the example of superconductivity, this would refer to the picture of preformed Cooper pairs. In Fig. 4, we show the simulated spectra for preformed Cooper pairs as a function of the correlation length, see Supplementary Methods for details. While the subtle back-bending behavior and its momentum alignment with K_F are satisfied for all correlation lengths (Fig. 4a), a smaller magnitude of the gap and a weaker quasiparticle peak are clearly associated with a shorter correlation length (Fig. 4b). The fully gapped spectrum with a sharp quasiparticle peak appears when the correlation length becomes much longer. If we assume that the correlation length in the real material becomes longer at lower temperatures, then the above simulation would also be qualitatively consistent with the temperature evolution of the spectra observed in our experiment (Fig. 2). We note that the simple simulation might not fully capture the complexity of the strongly correlated system, but the overall agreement suggests the preformed Cooper pairs as a viable mechanism for the observed pseudogap state of electron-doped Sr_2IrO_4.

However, a key question of whether the electron-doped Sr_2IrO_4 becomes superconducting at low temperature remains unresolved. Since the highest bulk electron doping level in Sr_2IrO_4 is still limited, potassium surface doping has been used to significantly enhance the electron doping level. However, transport measurements on potassium surface-doped samples remain a technical challenge. An earlier study reported a d-wave gap on

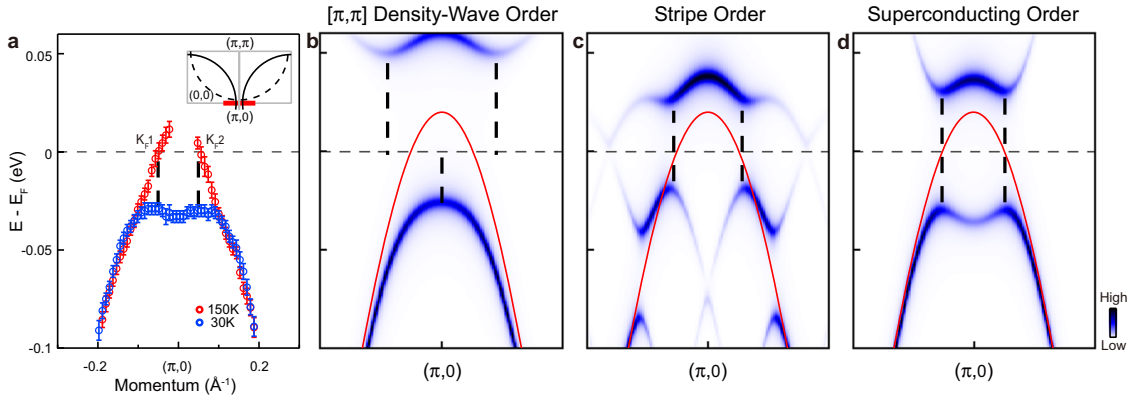

Fig. 3 Comparison of different electronic orders. a Experimental dispersion in the normal and gapped states. **b**–**d**, Simulated spectra for commensurate [π, π] density-wave order (**b**), stripe order with a wave vector connecting K_F1 and K_F2 (**c**) and superconducting order (**d**). Red curves represent the bare band in the simulation. Black dashed lines mark the back-bending momenta in the gapped states.

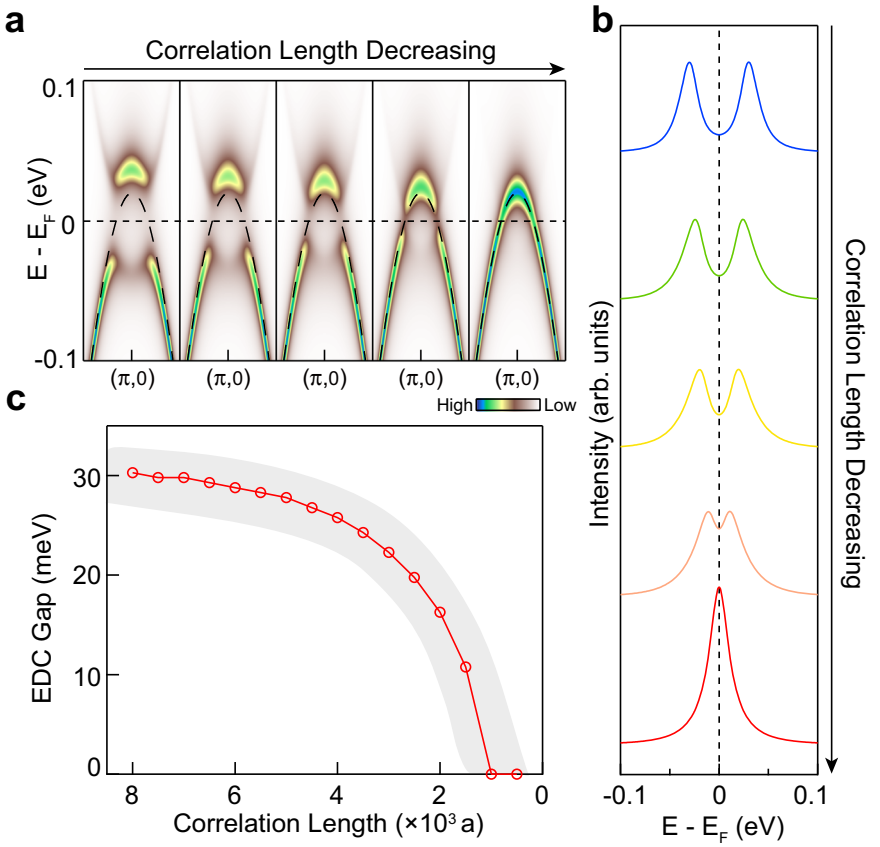

Fig. 4 Simulation of preformed Cooper pairs as a function of the correlation length. a Simulated spectra with selected correlation lengths ($\xi = 8000$, 3500, 2500, 1500 and 500 lattice parameter). The dashed black curves represent the bare band in the simulations. **b** EDC at the Fermi momentum, as a function of correlation length. **c** Gap magnitude as a function of correlation length, extracted from the simulated EDC at the Fermi momentum. Note that the absolute value of the correlation length in the simplified model cannot be directly compared with that in the real material, see Supplementary Methods for details.

potassium surface-doped Sr_2IrO_4 samples[16], where the gap near the node closes at ~30 K. In our measurements, the pseudogap in the antinodal region closes between 120 and 150 K. These results seem to be analogous to those in the underdoped cuprates[28]. In this sense, it would also be interesting to explore whether other special electronic orders may play a role. Notably, an incommensurate spin density wave with a relatively high transition temperature has been reported in electron-doped Sr_2IrO_4 samples[18]. It has been reported that an incommensurate charge density wave order in transition-metal dichalcogenides induces little change on the band dispersion but significantly contributes to the pseudogap[29,30]. In this sense, some incommensurate density wave orders are very difficult to identify by ARPES. Whether such a phenomenon would take place in electron-doped Sr_2IrO_4 remains to be understood. Also, preformed Cooper pairs and competing orders may coexist in the cuprates, but dominate

in different regions of the phase diagram[31]. The extent to which similar phenomena may be at play in the iridates remains to be explored.

Finally, we comment on the gapless normal state of electron-doped Sr_2IrO_4. While the band dispersion shows clear Fermi crossings at high temperature (Fig. 1a, c), the quasiparticle peak near E_F is very weak (Fig. 1a, c; Supplementary Fig. 8). Notably, a similar phenomenon has been observed in iron-based superconductors, where the energy gap closes at high temperature but no quasiparticle peak is present in the normal state[32]. A transition from the coherent quasiparticle to an incoherent strange metal has also been reported in the normal state of cuprates[31]. While the mechanism is still under debate, the disappearance of a well-defined quasiparticle points to a non-Fermi liquid behavior of the normal state.

Our study shows that the pseudogap state of the electron-doped Sr_2IrO_4 is consistent with the appearance of a short-range order with zero scattering wave vector. For such an order, the particle–hole symmetric preformed Cooper pairs represent a viable mechanism that has been identified over a wide doping range in the cuprates[3–5,11,31]. If these incoherent Cooper pairs underlie the pseudogap state of electron-doped Sr_2IrO_4 then superconductivity will likely be driven by the appearance of phase coherence in the system. It will also be interesting to explore whether other unknown orders could be at play with the experimentally identified properties. Further investigation of such an order and its relationship with the incoherent gapless normal state and superconductivity will help unravel the generic physics of doped spin-1/2 Heisenberg antiferromagnetic Mott insulators beyond the material-specific properties of the cuprates.

METHODS

Sample growth

Single crystals of $(Sr_{1-x}La_x)_2IrO_4$ were grown via a platinum (Pt) crucible-based flux growth method as described in earlier studies[18]. The electron doping was realized by in situ surface potassium deposition on the La-doped sample $(Sr_{1-x}La_x)_2IrO_4$ with x~0.048.

ARPES measurement

The bulk La-doped sample was used as the starting point for the surface doping in order to avoid the possible charging effect of the bulk material during ARPES measurements. The sample was cleaved in situ at 150 K, with a base pressure of better than 3×10^{-11} Torr. ARPES measurements were carried out at Beamline 5-4 of the Stanford Synchrotron Radiation Lightsource (SSRL) of SLAC National Accelerator Laboratory using 25 eV photons with a total energy resolution of ~9 meV. The Fermi level was referenced to that of polycrystalline Au in electrical contact with the sample. Details of theoretical calculations are described in the Supplementary Methods.

DATA AVAILABILITY

All data generated or analyzed during this study are included in this published article (and its supplementary information files).

Received: 18 November 2021; Accepted: 14 May 2022;
Published online: 03 June 2022

REFERENCES

1. Damascelli, A., Hussain, Z. & Shen, Z.-X. Angle-resolved photoemission studies of the cuprate superconductors. *Rev. Mod. Phys.* **75**, 473–541 (2003).
2. Sobota, J. A., He, Y. & Shen, Z.-X. Angle-resolved photoemission studies of quantum materials. *Rev. Mod. Phys.* **93**, 025006 (2021).
3. Kanigel, A. et al. Evidence for pairing above the transition temperature of cuprate superconductors from the electronic dispersion in the pseudogap phase. *Phys. Rev. Lett.* **101**, 137002 (2008).
4. Yang, H.-B. et al. Emergence of preformed Cooper pairs from the doped Mott insulating state in $Bi_2Sr_2CaCu_2O_{8+\delta}$. *Nature* **456**, 77–80 (2008).
5. Nakayama, K. et al. Evolution of a pairing-induced pseudogap from the superconducting gap of $(Bi, Pb)_2Sr_2CuO_6$. *Phys. Rev. Lett.* **102**, 227006 (2009).
6. Comin, R. & Damascelli, A. Resonant X-Ray scattering studies of charge order in cuprates. *Annu. Rev. Condens. Matter Phys.* **7**, 369–405 (2016).
7. Tanaka, K. et al. Distinct Fermi-momentum-dependent energy gaps in deeply underdoped Bi2212. *Science* **314**, 1910–1913 (2006).
8. Lee, W. S. et al. Abrupt onset of a second energy gap at the superconducting transition of underdoped Bi2212. *Nature* **450**, 81–84 (2007).
9. Kondo, T. et al. A. Competition between the pseudogap and superconductivity in the high-T_c copper oxides. *Nature* **457**, 296–300 (2009).
10. Hashimoto, M. et al. Particle-hole symmetry breaking in the pseudogap state of Bi2201. *Nat. Phys.* **6**, 414–418 (2010).
11. Vishik, I. M. Photoemission perspective on pseudogap, superconducting fluctuations, and charge order in cuprates: a review of recent progress. *Rep. Prog. Phys.* **81**, 062501 (2018).
12. Kim, Y. K. et al. Fermi arcs in a doped pseudospin-1/2 Heisenberg antiferromagnet. *Science* **345**, 187–190 (2014).
13. de la Torre, A. et al. Collapse of the Mott gap and emergence of a nodal liquid in lightly doped Sr_2IrO_4. *Phys. Rev. Lett.* **115**, 176402 (2015).
14. Wang, F. & Senthil, T. Twisted Hubbard Model for Sr_2IrO_4: magnetism and possible high temperature Superconductivity. *Phys. Rev. Lett.* **106**, 136402 (2011).
15. Watanabe, H., Shirakawa, T. & Yunoki, S. Monte Carlo study of an unconventional superconducting phase in iridium oxide J_{eff}=1/2 Mott insulators induced by carrier doping. *Phys. Rev. Lett.* **110**, 027002 (2013).
16. Kim, Y. K., Sung, N. H., Denlinger, J. D. & Kim, B. J. Observation of a d-wave gap in electron-doped Sr_2IrO_4. *Nat. Phys.* **12**, 37–41 (2016).
17. Yan, Y. J. et al. Electron-doped Sr_2IrO_4: an analogue of hole-doped cuprate superconductors demonstrated by scanning tunneling microscopy. *Phys. Rev. X* **5**, 041018 (2015).
18. Chen, X. et al. Unidirectional spin density wave state in metallic $(Sr_{1-x}La_x)_2IrO_4$. *Nat. Commun.* **9**, 103 (2018).
19. Battisti, I. et al. Universality of pseudogap and emergent order in lightly doped Mott insulators. *Nat. Phys.* **13**, 21–25 (2017).
20. Hu, Y. et al. Spectroscopic evidence for electron-boson coupling in electron-doped Sr_2IrO_4. *Phys. Rev. Lett.* **123**, 216402 (2019).
21. Cao, G. & Schlottmann, P. The challenge of spin-orbit-tuned ground states in iridates: a key issues review. *Rep. Prog. Phys.* **81**, 042502 (2018).
22. Bertinshaw, J., Kim, Y. K., Khaliullin, G. & Kim, B. J. Square lattice iridates. *Annu. Rev. Condens. Matter Phys.* **10**, 315–336 (2019).
23. Kim, B. J. et al. Novel J_{eff}=1/2 Mott state induced by relativistic spin–orbit coupling in Sr_2IrO_4. *Phys. Rev. Lett.* **101**, 076402 (2008).
24. Chu, H. et al. A charge density wave-like instability in a doped spin-orbit-assisted weak Mott insulator. *Nat. Mater.* **16**, 200–203 (2017).
25. Wang, Z. et al. Doping induced Mott collapse and possible density wave instabilities in $(Sr_{1-x}La_x)_3Ir_2O_7$. *npj Quantum Mater.* **4**, 43 (2019).
26. Kondo, T., Takeuchi, T., Tsuda, S. & Shin, S. Electrical resistivity and scattering processes in $(Bi, Pb)_2(Sr, La)_2CuO_{6+\delta}$ studied by angle-resolved photoemission spectroscopy. *Phys. Rev. B* **74**, 224511 (2006).
27. Norman, M. R., Randeria, M., Ding, H. & Campuzano, J. C. Phenomenology of the low-energy spectral function in high-T_c superconductors. *Phys. Rev. B* **57**, R11093 (1998).
28. Bilbro, L. S. et al. Temporal correlations of superconductivity above the transition temperature in $La_{2-x}Sr_xCuO_4$ probed by terahertz spectroscopy. *Nat. Phys.* **7**, 298–302 (2011).
29. Borisenko, S. V. et al. Pseudogap and charge density waves in two dimensions. *Phys. Rev. Lett.* **100**, 196402 (2008).
30. Borisenko, S. V. et al. Two energy gaps and fermi-surface "Arcs" in $NbSe_2$. *Phys. Rev. Lett.* **102**, 166402 (2009).
31. Chen, S.-D. et al. Incoherent strange metal sharply bounded by a critical doping in Bi2212. *Science* **366**, 1099–1102 (2019).
32. Huang, J. et al. Emergence of superconductivity from fully incoherent normal state in an iron-based superconductor $(Ba_{0.6}K_{0.4})$ Fe_2As_2. *Sci. Bull.* **64**, 11–19 (2019).

ACKNOWLEDGEMENTS

The authors thank M. Matzelle and Z. Y. Wang for useful discussions. The work at the university of science and technology of China (USTC) was supported by the National Natural Science Foundation of China (No. 12074358 and No. 12004363), the Fundamental Research Funds for the Central Universities No. WK3510000008 and No. WK2030000035, and the USTC start-up fund. Use of the Stanford Synchrotron Radiation Lightsource, SLAC National Accelerator Laboratory, is supported by the U.S. Department of Energy, Office of Science, Office of Basic Energy Sciences under

Contract No. DE-AC02-76SF00515. SIMES research was supported by U.S. Department of Energy, Office of Science, Office of Basic Energy Sciences, Division of Material Science. S.D.W. and X.C. acknowledge support from NSF Award No. DMR-1905801. The work at Northeastern University was supported by the US DOE, Office of Science, Basic Energy Sciences grant number DE-FG02-07ER46352, and benefited from Northeastern University's Advanced Scientific Computation Center (ASCC) and the NERSC supercomputing center through DOE grant number DE-AC02-05CH11231. C.L. was supported by the U.S. DOE NNSA under Contract No. 89233218CNA000001 and by the Center for Integrated Nanotechnologies, a DOE BES user facility, in partnership with the LANL Institutional Computing Program for computational resources. Additional support was provided by DOE Office of Basic Energy Sciences Program E3B5. Y. W. acknowledges support from the National Science Foundation (NSF) award DMR-2132338.

AUTHOR CONTRIBUTIONS

S.P., C.L., Y.H., and M.G. contributed equally to this work. J.H. proposed and designed the research. J.H., Y.H., and S.P. carried out the ARPES measurements and analyzed the data. C.L., M.G., S.P., R.S.M., Y.W., and A.B. performed the calculations and provided theoretical guidance. X.C. grew the samples with support from S.D.W. X.C., S.P., and Z.S. characterized the samples with support from S.D.W., T.W. and X.-H.C. M. H., and D.L. maintained the ARPES facilities at SSRL with support from Z.-X.S. S.P., and J.H. wrote the paper with inputs from all authors.

COMPETING INTERESTS

The authors declare no competing interests.

ADDITIONAL INFORMATION

Supplementary information The online version contains supplementary material available at https://doi.org/10.1038/s41535-022-00467-1.

Correspondence and requests for materials should be addressed to Junfeng He.

Reprints and permission information is available at http://www.nature.com/reprints

Publisher's note Springer Nature remains neutral with regard to jurisdictional claims in published maps and institutional affiliations.